

WIND-ACCRETION DISKS IN WIDE BINARIES, SECOND GENERATION PROTOPLANETARY DISKS AND ACCRETION ONTO WHITE DWARFS

HAGAI B. PERETS¹ AND SCOTT J. KENYON²

¹Deloro fellow, Technion - Israel Institute of Technology, Haifa, Israel

²Harvard-Smithsonian Center for Astrophysics, 60 Garden St., Cambridge, MA, USA 02138

Draft version June 17, 2018

Abstract

Mass transfer from an evolved donor star to its binary companion is a standard feature of stellar evolution in binaries. In wide binaries, the companion star captures some of the mass ejected in a wind by the primary star. The captured material forms an accretion disk. Here, we study the evolution of wind-accretion disks, using a numerical approach which allows us to follow the long term evolution. For a broad range of initial conditions, we derive the radial density and temperature profiles of the disk. In most cases, wind-accretion leads to long-lived stable disks over the lifetime of the AGB donor star. The disks have masses of a few times $10^{-5} - 10^{-3} M_{\odot}$, with surface density and temperature profiles that follow broken power-laws. The total mass in the disk scales approximately linearly with the viscosity parameter used. Roughly 50% to 80% of the mass falling into the disk accretes onto the central star; the rest flows out through the outer edge of the disk into the stellar wind of the primary. For systems with large accretion rates, the secondary accretes as much as $0.1 M_{\odot}$. When the secondary is a white dwarf, accretion naturally leads to nova and supernova eruptions. For all types of secondary star, the surface density and temperature profiles of massive disks resemble structures observed in protoplanetary disks, suggesting that coordinated observational programs might improve our understanding of uncertain disk physics.

1. INTRODUCTION

Mass transfer from an evolved donor star to a companion star is a common outcome of stellar evolution in binary systems. In close binaries with periods of 1–2 yr or less, the donor can fill its tidal surface and transfer mass rapidly into a massive disk surrounding the companion (e.g., Kenyon et al. 1982; Bath & Pringle 1982b; Kenyon et al. 1991; Siviero et al. 2009). Although these disks are luminous, the systems are short-lived and rarely observable (Kenyon & Webbink 1984; Kenyon 1986).

Disks formed via wind accretion may be more common. Chemically peculiar stars, including Barium stars and CH stars, are probably polluted by material accreted from a binary companion (McClure & Woodsworth 1990; Luck & Bond 1991; Han et al. 1995; Busso et al. 2001). White dwarfs (WDs) accreting material through disks filled by the winds of their evolved companions are often identified as symbiotic stars or very slow (also symbiotic) novae (Kenyon & Truran 1983; Kenyon 1986; Webbink et al. 1987; Sokoloski et al. 2006). In both cases, long-lived disks are possible when the donor star does not fill its tidal lobe.

Theoretical studies of the physical properties of wind-accretion disks provide an important framework for interpreting observations of these systems. The replenishment of newly accreted material and the formation of a disk may also have important implications for the formation and evolution of planetary systems. A newly formed disk may interact with pre-existing planets, leading to the re-growth and/or migration of these planets, or possibly the formation new planets and/or debris disks (Perets 2010a,b).

Several previous studies explored the formation of

wind-accretion disks through SPH and AMR simulations (Mastrodemos & Morris 1998; de Val-Borro et al. 2009). Here we use a different simplified analytical/numerical approach typically used for the study of disks in shorter period binaries and in protostellar/protoplanetary systems. This approach allows us to follow the long term evolution of the disks, which is more difficult in hydro simulations, and to compare the derived physical structure with protoplanetary disks. We focus on the accretion from low mass companions in wide binaries (3 – 100 AU), which evolve through wind-accretion.

We begin with a description of the basic conditions in wind-accreting binaries, followed by a detailed explanation of the methods we use to follow their evolution. We then describe results of the wind-accretion disk structure followed by a discussion and summary.

2. WIND ACCRETION IN WIDE BINARIES

To understand the conditions required for the formation of circumstellar disks from wind accreted material, we follow Soker & Rappaport (2000). For a disk to form, j_a , the specific angular momentum of the accreted material, must exceed $j_2 = (GM_2R_2)^{1/2}$, the specific angular momentum of a particle in a Keplerian orbit at the equator of the accreting star of radius R_2 . For accretion from a wind, the net specific angular momentum of the material entering the Bondi-Hoyle accretion radius, R_a , is $j_{BH} = 0.5(2\pi/P)R_a^2$ (Wang 1981), where P is the orbital period. The actual accreted specific angular momentum for high Mach number flows is $j_a = \eta j_{BH}$, where $\eta \sim 0.1$ and $\eta \sim 0.3$ for isothermal and adiabatic flows, respectively (Livio et al. 1986). For a binary composed of a main sequence (MS) accretor with mass M_2 and a mass-losing asymptotic giant branch (AGB) star with mass M_1 , requiring $j_a > j_2$ leads to a simple condition for

disk formation

$$1 < \frac{j_a}{j_2} \simeq 1.2 \left(\frac{\eta}{0.2} \right) \left(\frac{M_1 + M_2}{2.5M_\odot} \right) \left(\frac{M_2}{M_\odot} \right)^{3/2} \\ \times \left(\frac{R_2}{R_\odot} \right)^{-1/2} \left(\frac{a}{100\text{AU}} \right)^{-3/2} \left(\frac{v_r}{10\text{km s}^{-1}} \right)^{-4} \quad (1)$$

where R_2 is the radius of the accreting star, a is the semi-major axis of the binary, and v_r is the relative velocity of the wind and the accretor.

Adopting $R_2 \sim R_\odot$, disks can form in binaries with $a \lesssim 10\text{--}100$ AU for $M_1 \approx 1\text{--}10 M_\odot$ and $v_r \approx 5\text{--}20 \text{ km s}^{-1}$. This range in a spans the peak of the distribution of binary star separations (Duquennoy & Mayor 1991). Thus, many binaries contain wind-accretion disks during the late stages of their evolution.

Red giant branch (RGB) and AGB stars lose mass in low velocity winds at typical rates of $\dot{M}_w \sim 10^{-8}\text{--}10^{-5} M_\odot \text{ yr}^{-1}$ (e.g., Taylor & Seaquist 1984; Kenyon 1986; Olofsson et al. 2002; Ramstedt et al. 2006). To estimate the fraction of this material accreted by the MS companion, we adopt the Bondi-Hoyle rate for an isotropic wind from the mass-losing star,

$$\dot{M}_a = \left(\frac{R_a}{2a} \right)^2 \dot{M}_w, \quad (2)$$

where R_a is the Bondi-Hoyle accretion radius

$$R_a = \frac{2GM_2}{v_r^2 + c_s^2}. \quad (3)$$

In this expression, $v_r^2 = v_w^2 + v_o^2$ is the velocity of wind material near the secondary, v_o is the orbital velocity of the secondary, and c_s is the sound speed of the wind. For typical velocities of $\sim 10\text{--}20 \text{ km s}^{-1}$, \dot{M}_a/\dot{M}_w ranges from $\sim 20\%$ for close binaries with $a \approx 3$ AU, to $\lesssim 0.1\%$ for wider binaries with $a \approx 100$ AU. Thus, maximum accretion rates can briefly reach roughly $10^{-5} M_\odot \text{ yr}^{-1}$ for close binaries with AGB star companions.

Despite the relatively low efficiency, wind accretion can add considerable mass to the secondary. While on the RGB and AGB, the primary star loses most of its initial mass. For primaries with initial masses $1\text{--}7 M_\odot$, close companions can accrete as much as $1 M_\odot$ from wind accretion.

Detailed AMR simulations of wind-accretion disks yield results consistent with these simple estimates (de Val-Borro et al. 2009). When the star serves as a sink term in the simulations, circumstellar material forms a fairly stable disk with a total mass of $\sim 10^{-4}$ of the stellar mass out to radii of roughly 5 AU. Typically, $\sim 5\%$ of the mass lost from the AGB star goes through the disk, consistent with the simple Bondi-Hoyle estimates.

To develop a model for the structure of the disk, we assume the primary loses mass at a constant rate, \dot{M}_w . For wide binaries, wind material is ejected far from the accretor at approximately parallel trajectories. Gravitational focusing close to the accretor then sets the cross-section for material hitting the disk. Instead of the geometrical cross-section, the fraction of the wind captured by the disk up to distance r is $f_{\dot{M}_{acc}}(< r) \propto r$. For an outer

radius equal to R_a ,

$$f_{\dot{M}_{acc}}(< R) = \frac{R}{R_a}. \quad (4)$$

The differential accretion rate per radial bin in the disk, is therefore

$$\dot{M}_{acc}(R)dR = \dot{M}_{acc}^{tot} \frac{dR}{R_a}. \quad (5)$$

The source function, the instantaneous surface density profile of material accreted into the disk is

$$\dot{\Sigma}_S(R)dR = \frac{\dot{M}_{acc}(R)}{2\pi R} = \frac{\dot{M}_{acc}^{tot} dR}{2\pi R R_a}. \quad (6)$$

As wind material falls into the disk, it dissipates kinetic energy. Together with irradiation from the central star and viscous heating, this energy contributes to the heating of the disk. The amount of energy input into an annulus at radius r is the gravitational binding energy,

$$\dot{E}_S(R)dR = \frac{GM_2 \dot{M}_{acc}^{tot} dR}{R R_a}. \quad (7)$$

Although the disk does not accrete material beyond R_a , viscous processes can expand the disk beyond R_a . However, tidal forces from the binary companion limit the outer radius. Typically, this outer radius is roughly 90% to 95% of the Roche limit, $a_2 = r_1 a$, where

$$r_1 = \frac{0.49q^{2/3}}{0.6q^{2/3} + \ln(1 + q^{1/3})} \quad (8)$$

and $q = M_2/M_1$ (Eggleton 1983).

For wind mass loss with $M_1 > M_2$ and low accretion efficiency, binaries expand. We approximate this expansion assuming adiabatic mass loss from the primary star (Hadjidemetriou 1963)

$$a(t) = \frac{M_{1,init} + M_{2,init}}{M_1(t) + M_2(t)} a_{init}, \quad (9)$$

where $M_{i,init}$ are the initial masses of the binary components, a_{init} is the initial separation and

$$M_i(t) = M_{i,init} + \int_0^t \dot{M}_i(t) dt, \quad (10)$$

for $i = 1, 2$. Assuming a constant mass loss rate from the primary, $M_1(t) = M_{1,init} - \dot{M}_w t$ and $M_2(t) = M_{2,init} + \zeta \dot{M}_w t$, where ζ is the accretion efficiency. For a system losing mass in a wind ($\zeta \ll 1$), $a(t) > a_{init}$. Thus, the binary separation expands with time. For most mass loss rates and separations of interest, the disk reaches a steady-state on timescales shorter than the lifetime of the AGB star (see results in Table 1). Thus, we can safely adopt a simple prescription for the outer radius of the disk

$$R_{out} = a_2 \quad (11)$$

and assume that a is constant in time. Considering a broad range of a and \dot{M}_w allows us to derive conditions in the disk for a broad range of plausible binaries (see Table 1).

The inner boundary of the disk, R_{in} , is limited by the radius of the accreting star

$$R_{in} = R_2; \quad (12)$$

we adopt an inner radius of $1.5R_2$; the precise value of the inner radius has little impact on the overall structure of the wind-filled accretion disk.

Equipped with the necessary initial and boundary conditions, we now discuss a model for the evolution of the disk.

3. DISK EVOLUTION

3.1. Numerical calculation

For a disk with surface density Σ and viscosity ν , conservation of angular momentum and energy leads to a non-linear diffusion equation for the time evolution of Σ (e.g., Lynden-Bell & Pringle 1974; Pringle 1981),

$$\frac{\partial \Sigma}{\partial t} = 3R^{-1} \frac{\partial}{\partial R} \left(R^{1/2} \frac{\partial}{\partial R} \{ \nu \Sigma R^{1/2} \} \right) + \left(\frac{\partial \Sigma}{\partial t} \right)_{ext}. \quad (13)$$

The first term is the change in Σ from viscous evolution; the second term is the change in Σ from other processes, including mass loss from photoevaporation (e.g. Alexander et al. 2006) or planet formation (e.g., Alexander & Armitage 2009) and mass gain from wind material falling into the disk (given by Eq. 6). Our approach neglects the torque of the disk by the wind, which is small for a disk in a binary system. For the wide binaries we consider (30 and 100 AU separation), the wind momentum can compress the outer edges of the disk but does not affect its bulk structure. The viscosity is $\nu = \alpha c_s H$, where c_s is the sound speed, H is the vertical scale height of the disk, and α is the viscosity parameter. The sound speed is $c_s^2 = \gamma k T_d / \mu m_H$, where γ is the ratio of specific heats, k is Boltzmann's constant, T_d is the midplane temperature of the disk, μ is the mean molecular weight, and m_H is the mass of a hydrogen atom. The scale height of the disk is $H = c_s \Omega^{-1}$, where $\Omega = \sqrt{GM_\star / R^3}$ is the angular velocity.

To solve this equation numerically, we assume that the midplane temperature is the sum of the energy generated by viscous (T_v) dissipation, the energy from irradiation (T_I), and the energy of infalling material from the wind (T_W),

$$T_d^4 = T_v^4 + T_I^4 + T_W^4. \quad (14)$$

The viscous temperature is

$$T_v^4 = \frac{27\kappa\nu\Sigma^2\Omega^2}{64\sigma}, \quad (15)$$

where κ is the opacity and σ is the Stefan-Boltzmann constant (e.g. Ruden & Lin 1986; Ruden & Pollack 1991). With $\nu = \alpha c_s^2 \Omega^{-1}$ and $t_2 = (27\alpha/64\sigma) \sim (\gamma k / \mu m_H) \sim \kappa \Omega \Sigma^2$, the viscous temperature is

$$T_v^4 = t_2 T_d. \quad (16)$$

The energy from infalling material follows from Eq. 7. Balancing the kinetic energy of infall with the energy radiated by the disk yields

$$\sigma 2\pi R d R T_W^4(R) = \frac{GM_2 \dot{M}_{acc} d R}{R R_a}. \quad (17)$$

Solving this equation for T_W requires

$$\sigma T_W^4 = \frac{GM_2 \dot{M}_{acc}}{2\pi R^2 R_a}. \quad (18)$$

If the disk is vertically isothermal, the irradiation temperature is $T_I^4(R) = (\theta/2)(R_\star/R)^2 T_\star^4$, where R_\star and T_\star are the radius and effective temperature of the central star and (Chiang & Goldreich 1997)

$$\theta = \frac{4}{3\pi} \left(\frac{R_\star}{R} \right)^3 + R \frac{\partial(H/R)}{\partial R}. \quad (19)$$

Thus, the irradiation temperature is

$$\left(\frac{T_I}{T_\star} \right)^4 = \frac{2}{3\pi} \left(\frac{R_\star}{R} \right)^3 + \frac{H}{2R} \left(\frac{R_\star}{R} \right)^2 \left(\frac{\partial \ln H}{\partial \ln R} - 1 \right). \quad (20)$$

Following Chiang & Youdin (2010) and Hueso & Guillot (2005), we set $\partial \ln H / \partial \ln R = 9/7$. With $H = c_s \Omega^{-1}$, we set $t_0 = (2T_\star/3\pi)(R_\star/R)^3$ and $t_1 = (R_\star/R)^2 \sim (7R\Omega)^{-1} \sim (\gamma k / \mu m_H)^{1/2} \sim T_\star$. The irradiation temperature is then

$$T_I^4 = t_0 + t_1 T_d^{1/2}. \quad (21)$$

Viscous disks are not vertically isothermal (Ruden & Pollack 1991; D'Alessio et al. 1998); however this approach yields a reasonable approximation to the actual disk structure.

Because T_v and T_I are functions of the midplane temperature, and T_W is independent of it, we solve equation (14) with a Newton-Raphson technique. Using equations (16), (21), and 18, we re-write equation (14) as

$$f(T_d) = T_d^4 - (t_0 + t_1 T_d^{1/2} + t_2 T_d + T_W) = 0. \quad (22)$$

Adopting an initial $T_d \approx t_2^{1/3}$ or $T_d \approx t_1^{2/7}$, the derivative

$$\frac{\partial f}{\partial T_d} = 4T_d^3 - \frac{t}{2} T_d^{-1/2} - t_2 \quad (23)$$

allows us to compute

$$\delta T_d = f \left(\frac{\partial f}{\partial T_d} \right)^{-1} \quad (24)$$

and yields a converged T_d to a part in 10^8 in 2-3 iterations.

In the inner disk, the temperature is often hot enough to vaporize dust grains. To account for the change in opacity, we follow Chambers (2009) and assume

$$\kappa = \kappa_0 \left(\frac{T_d}{T_e} \right)^n \quad (25)$$

with $n = -14$ in regions with $T_d > T_e = 1380$ K (Ruden & Pollack 1991; Stepinski 1998). For simplicity, we assume $\kappa = \kappa_0$ when $T_d < T_e$.

To solve for the time evolution of Σ , we use an explicit technique with N annuli on a grid extending from x_{in} to x_{out} where $x = 2 R^{1/2}$ (Bath & Pringle 1981, 1982a), and R_{in} and R_{out} are inner and outer boundaries determined by Eqs. 11. To verify this code, Bromley & Kenyon (2011) compare numerical solutions with analytic results from Chambers (2009).

3.2. Potential caveats

Our study explores wind-accretion disks using simple numerical models. These models provide us with the ability to explore the long term evolution of disks with a wide range of initial conditions. Because these disks reach an approximate steady-state, we can test whether the solutions scale as expected with the binary separation and the mass loss rate of the primary star. However, the approach makes many simplifying assumptions, and does not consider many physical processes known to occur in these systems. Because the physics we do not include is often poorly understood or weakly constrained, it seems prudent to begin with a simple physical structure and add additional physics as needed to understand a broader range of phenomena. The following paragraphs discuss useful physics to consider for future studies.

Radiative heating of the disk by the companion: Our calculations do not include radiative heating of the disk by the primary star (mass donor). If the primary has a radius $R_1 \approx 0.5$ AU and a luminosity L_1 , a flared disk surrounding the secondary with outer radius R_{out} and vertical scale height $h_{out} \approx 0.05 R_{out}$ intercepts 0.4% to 0.01% of L_1 for $a = 3$ –100 AU (Kenyon & Hartmann 1987). With $L_1 \approx 500$ –1000 L_\odot , this contribution to disk heating is comparable to irradiation by the central MS star. In wide binaries with $a \approx 10$ –100 AU, AGB stars can have $R_1 \approx 1$ AU. The disk then intercepts 0.2% ($a = 10$ AU) to 0.02% ($a = 100$ AU) of the radiation from the primary. For typical AGB $L_1 \sim 10^4 L_\odot$ and $a \approx 10$ AU, this component is somewhat larger than irradiation from the central star. In all configurations, the outer rim of the disk intercepts nearly all of this radiation. If the outer disk radiates efficiently, this extra heating should not impact the structure of material in the inner disk. To test this assumption, we performed several test simulations with a fixed outer boundary temperature, $\sigma T_{out}^4 = f_{irr} L_1 / 4\pi R_{out} h_{out}$. This extra heating reduces the disk surface density by a factor of ~ 2 near the outer boundary but changes the surface density at smaller radii, $R \lesssim 0.95 R_{out}$, by less than 1%. Thus, neglecting this component has little impact on our results. If the outer disk radiates inefficiently, the outer disk will expand and transport thermal energy radially inward. If the scale height of this puffed up disk becomes comparable to the accretion radius R_a it could significantly affect the accretion process, and would require a different approach.

Disk viscosity: The processes underlying the origin of the viscosity in accretion disks are still not understood. Here, we follow most studies and adopt a simple prescription using the α viscosity parameter. In particular, we do not directly consider here any interactions of magnetic fields and their evolution, and we use a constant α in each model. Our general results are shown for our choice of $\alpha = 0.01$. Table 1 also provides additional data for the cases of $\alpha = 0.001$ and $\alpha = 0.1$, enabling us to consider the overall dependence of disk structure and evolution on the viscosity parameter.

Binary orbital expansion: As briefly discussed above, we do not change the binary separation and mass in our calculation. In most cases the wind-accretion disk evolves to a steady state in a relatively short time scale. Our approach then provides a good approximation to re-

ality. When evolution in the binary separation occurs more rapidly than the time-scale to reach steady-state conditions in the disk (e.g., when the time-scale to reach steady-state is $\gtrsim 10^5$ yr), our approximation is less accurate. Our results should then be taken with more caution. In general, both the evolution of the binary and the equilibrium disk mass evolve slowly enough to treat the time evolution with a sequence of steady disk models in binaries with increasing semi-major axis.

Accretion model and disk instabilities: We use a simplified 1D model for the accretion infall of wind material into the disk. Although this model captures many of the main properties of the material infall, reality is probably more complex. Aside from our failure to treat the complex interaction between the wind and the outer disk, our simplified 1.5D model does not allow for variations in the vertical structure which might lead to thermal instabilities and dwarf nova outbursts (e.g., Cannizzo et al. 2012, and references therein) or for winds driven by radiation pressure from the inner disk (e.g., Noebauer et al. 2010). In particular, the inner region where the temperatures rise above 1000–2000 K, (roughly where dust grains evaporate) might become thermally unstable (see e.g. Alexander et al. 2011). Though the location of the disk instability regime depends on the opacity model, the mass loss rate of the AGB primary, and other input parameters, Fig. 3 shows that temperatures as high as 1000 K are typically achieved only for a small region, extending up to an AU for the models with the highest accretion rate and/or the smallest binary separations. In most models, these relatively high temperatures are achieved only over small regions in the inner 0.1–0.3 AU of the disk. In models with the smallest binary separation (3 AU), the outer disk radius is comparable to disks studied in other contexts (e.g., Alexander et al. 2011). In wider binaries with separations of 10–100 AU, the outer disk extends well beyond regions likely capable of sustaining a thermal instability cycle. Thus, potentially unstable regions can extend over a large fraction of the disk in compact binaries ($a \approx 3$ AU) but impact a fairly small fraction of the disk in wider binaries ($a \gtrsim 10$ –100 AU). We therefore conclude that models exploring small separations, particularly those with the highest accretion rates (e.g. models 1 and 5 in table 1 below), could be highly susceptible to disk instabilities in a significant fraction of the inner disk. We caution that our steady state solutions might not well represent these cases. The steady state solution is likely to well represent likely outcomes in wider binaries and in compact binaries with low accretion rates. In all cases, likely unstable regions are close to the accreting star and could lead to outbursts with distinct observational outcomes. In Alexander et al. (2011), the optical brightness changes little during the outbursts; the bolometric luminosity changes by a relatively small factor of a few for the largest infall rates, though these are larger than those we study.

4. RESULTS

To develop an understanding of the long term behavior of wind-fed disks in wide binaries, we consider a grid of models in (a, \dot{M}_{wind}) space (see Tables 1 and 2 for model parameters and results). For simplicity, we adopt $q = 3$, $M_2 = 1 M_\odot$ (MS secondary) or $M_2 = 0.6 M_\odot$ (WD secondary), and assume constant separation and mass

loss rate with time. For each (a, \dot{M}_{wind}) pair, we set $v_w = 10 \text{ km s}^{-1}$ and $c_s = 20 \text{ km s}^{-1}$, derive R_a from equation (3) and R_{out} from equation (11). The disk inner cut-off is $R_{in} = 1.4R_2$, with $R_2 = 1 R_\odot$ for the main sequence stars and $R_2 = 0.01 R_\odot$ for the white dwarf stars.

For an initial disk mass $M_{d,0} = 10^{-7} M_\odot$, the initial surface density distribution is $\Sigma = \Sigma_0 R^{-1} e^{-R/R_{out}}$ with $\Sigma_0 = M_{d,0}/2\pi R R_{out}$. Using our numerical solution to the diffusion equation, we continuously add material to the disk inside R_a and evolve the surface density in time until (and if) the disk reaches a steady state at time τ_{steady} , or up to 1–2 Myr, corresponding to the maximum lifetimes of AGB stars. As long as the steady-state disk mass M_{steady} is much larger than the initial disk mass, numerical tests show that the initial surface density distribution has little impact on the final steady-state surface density distribution.

We consider the system to reach a steady state when the change in disk mass per unit time is smaller than 10^{-3} of the input rate. In most cases, disks reach steady state on timescales much shorter than the AGB lifetimes (see Fig. 1). Several models with the largest binary separations do not properly fulfill this steady state condition by the end of the simulation, but the actual change in the disk structure at late times is small. For these models we show the disk properties at the end of the simulation run time, τ_{run} . In these cases, τ_{run} is already comparable or longer than the typical AGB lifetime. Thus, wind accretion disk cannot achieve a steady state configuration. Nevertheless the disk structure in these cases hardly changes over most of the AGB lifetime.

Tables 1–2 summarize the main results of the calculations. The detailed steady state profile and evolution of the disks and the accretion rate (on to the star) are shown in Figs. 1–3. Although we focus on main sequence star accretors in the Figures, results for WD accretors are similar. Table 2 shows results for white dwarfs with negligible luminosity. If the accreting star is a hot white dwarf with $L = 100 L_\odot$, UV photons heat up disk regions close to the central star but impact the outer disk very weakly. Thus, the time evolution of the accretion rate and disk mass (in Fig. 1) and the radial profiles of cumulative mass, surface density, and disk temperature (Figs. 2–5) are fairly representative of WD accretors and MS accretors.

For all calculations, the disk mass and the accretion rate onto the star increase roughly linearly with time and then reach an approximate steady state (Figure 1). The timescale to reach steady-state increases roughly linearly with increasing binary separation. Although the relation is shallower than a linear one, binaries with smaller mass infall rates also take longer to reach steady state than binaries with large mass infall rates. The steady state disk masses range from $\sim 10^{-3} M_\odot$ for binaries with massive winds and small separations to $\sim 10^{-7} M_\odot$ for binaries with low mass loss rates and large separations. For models with identical mass loss rates from the evolved companion, wider binaries have smaller infall rates into the disk and smaller disk masses. When binaries with different a have similar infall rates, wider binaries have larger and more massive disks.

For most main sequence star models, wind-fed accretion rates produce negligible luminosities. With typical

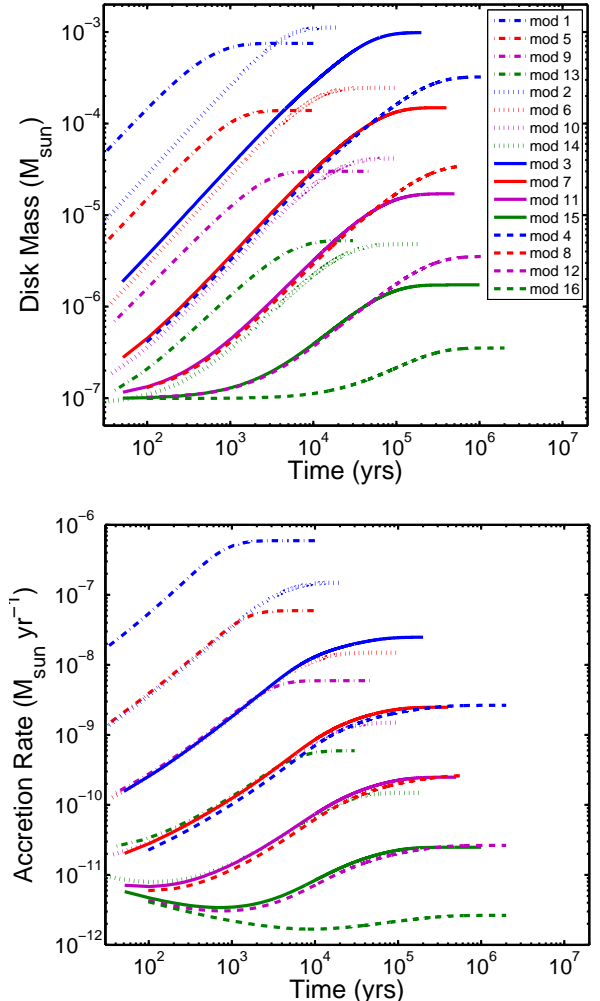


FIG. 1.— Disk mass profile and evolution. Top: The evolution of the total mass in the accretion disk. Disks in binaries with larger separations are wider and accommodate more mass, as they are truncated at further distances from the star. Bottom: Evolution of the accretion rate onto the star. Both upper figures show how the disk evolves into a steady state configuration over timescales which are typically much shorter than the mass loss time scales. The lines correspond to the models described in Table 1. Lines of the same color correspond to similar mass loss from the companion (10^{-5} , 10^{-6} , 10^{-7} and $10^{-8} M_\odot \text{ yr}^{-1}$ from top to bottom). Lines of the same type correspond to similar binary separation (3 AU, dash-dotted; 10 AU, dotted; 30 AU, solid; 100 AU, dashed).

steady accretion rates smaller than $10^{-7} M_\odot \text{ yr}^{-1}$, the accretion luminosity is comparable to or smaller than the stellar luminosity of $1 L_\odot$. Thus, the accretion disk and boundary layer are invisible (Kenyon & Webbink 1984). For close binaries with AGB-type primary stars, accretion rates of $10^{-6} M_\odot \text{ yr}^{-1}$ produce modest accretion luminosities of $\sim 10 L_\odot$. Although optical radiation from the disk and boundary layer are not detectable, ultraviolet (UV) radiation from the boundary layer is probably visible (Kenyon & Webbink 1984).

Models of wind-fed white dwarf stars are more interesting. In these systems, accretion rates exceeding $10^{-9} M_\odot \text{ yr}^{-1}$ yield bright UV sources which can ionize the wind from the primary (Kenyon & Webbink 1984). This ionized wind produces bright optical and UV emission lines (Kenyon & Webbink 1984) and a luminous ra-

TABLE 1
MS SECONDARY MODELS

# ¹	m_1 ²	m_2 ³	a ⁴	R_a ⁵	R_{out} ⁶	\dot{M}_{loss} ⁷	\dot{M}_{disk} ⁸	$\dot{M}_{disk}^{0.5}$ ⁹	\dot{M}_{in} ¹⁰	M_{disk}^{11}			τ_{steady}^{12}			τ_{run}^{13}		
										10^{-3}	10^{-2}	10^{-1}	10^{-3}	10^{-2}	10^{-1}	10^{-3}	10^{-2}	10^{-1}
1	3.0	1.0	3.0	1.5	1.4	-5.0	-5.74	-0.05	-6.23	-2.20	-3.12	-4.01	4.51	3.51	2.57	5.00	4.00	3.00
2	3.0	1.0	10.0	2.5	4.8	-5.0	-6.55	-0.85	-6.82	-2.12	-2.96	-3.77	5.08	4.28	3.51	5.30	4.30	3.70
3	3.0	1.0	30.0	3.1	14.3	-5.0	-7.46	-1.74	-7.60	-2.14	-3.00	-3.89	6.11	5.28	4.51	6.30	5.30	4.70
4	3.0	1.0	100.0	3.4	47.6	-5.0	-8.49	-2.80	-8.59	-2.53	-3.49	-4.47	6.97	6.30	5.00	6.97	6.30	5.30
5	3.0	1.0	3.0	1.5	1.4	-6.0	-6.74	-1.05	-7.23	-3.00	-3.85	-4.70	4.54	3.67	2.84	5.00	4.00	3.00
6	3.0	1.0	10.0	2.5	4.8	-6.0	-7.55	-1.85	-7.82	-2.77	-3.62	-4.49	5.51	4.66	3.83	6.00	5.00	4.00
7	3.0	1.0	30.0	3.1	14.3	-6.0	-8.46	-2.74	-8.60	-2.89	-3.82	-4.80	6.51	5.51	4.52	6.60	5.60	4.60
8	3.0	1.0	100.0	3.4	47.6	-6.0	-9.49	-3.80	-9.59	-3.47	-4.46	-5.46	7.00	6.00	5.04	7.23	6.00	5.30
9	3.0	1.0	3.0	1.5	1.4	-7.0	-7.74	-2.05	-8.23	-3.68	-4.52	-5.40	5.51	4.51	3.51	5.70	4.70	3.70
10	3.0	1.0	10.0	2.5	4.8	-7.0	-8.55	-2.85	-8.82	-3.47	-4.39	-5.34	5.83	4.96	4.04	6.00	5.00	4.30
11	3.0	1.0	30.0	3.1	14.3	-7.0	-9.46	-3.74	-9.60	-3.80	-4.77	-5.77	6.52	5.54	4.54	6.70	5.70	4.70
12	3.0	1.0	100.0	3.4	47.6	-7.0	-10.49	-4.80	-10.59	-4.46	-5.46	-6.46	7.04	6.04	5.00	7.30	6.30	5.30
13	3.0	1.0	3.0	1.5	1.4	-8.0	-8.74	-3.05	-9.23	-4.37	-5.28	-6.24	5.23	4.36	3.43	5.48	4.48	3.48
14	3.0	1.0	10.0	2.5	4.8	-8.0	-9.55	-3.85	-9.82	-4.34	-5.32	-6.32	6.04	5.04	4.04	6.30	5.30	4.30
15	3.0	1.0	30.0	3.1	14.3	-8.0	-10.46	-4.74	-10.60	-4.77	-5.77	-6.77	6.54	5.54	4.51	7.00	6.00	5.00
16	3.0	1.0	100.0	3.4	47.6	-8.0	-11.49	-5.80	-11.59	-5.46	-6.46	-7.46	7.04	6.00	5.04	7.30	6.30	5.30

Columns: (1) Model number; (2) Primary mass (M_\odot); (3) Secondary mass (M_\odot); (4) SMA separation (AU); (5) Bondi-Hoyle accretion radius (AU); (6) Outer boundary of the disk (AU); (7) Mass loss rate from primary ($M_\odot \text{ yr}^{-1}$); (8) Accretion rate into disk ($M_\odot \text{ yr}^{-1}$); (9) Total mass that goes through the disk in 0.5 Myrs (M_\odot); (10) Accretion rate onto the star ($M_\odot \text{ yr}^{-1}$); (11) Disk mass at steady state (M_\odot); (12) Time to achieve steady state (yrs); (13) Simulation run time (yrs). Columns 7-13 are shown in logarithmic scale.

TABLE 2
WD SECONDARY MODELS

# ¹	m_1 ²	m_2 ³	a ⁴	R_a ⁵	R_{out} ⁶	\dot{M}_{loss} ⁷	\dot{M}_{disk} ⁸	$\dot{M}_{disk}^{0.5}$ ⁹	\dot{M}_{in} ¹⁰	M_{disk} ¹¹	τ_{steady} ¹²	τ_{run} ¹³
1	1.8	0.6	3.0	1.2	1.4	-5.0	-6.06	-0.37	-6.47	-3.29	4.00	4.48
2	1.8	0.6	10.0	1.7	4.8	-5.0	-6.96	-1.26	-7.18	-3.24	4.51	4.70
3	1.8	0.6	30.0	2.0	14.3	-5.0	-7.89	-2.19	-8.02	-3.25	5.51	5.70
4	1.8	0.6	100.0	2.1	47.6	-5.0	-8.96	-3.24	-9.00	-3.51	6.30	6.30
5	1.8	0.6	3.0	1.2	1.4	-6.0	-7.06	-1.37	-7.47	-4.00	3.75	4.00
6	1.8	0.6	10.0	1.7	4.8	-6.0	-7.96	-2.26	-8.18	-3.85	4.80	5.00
7	1.8	0.6	30.0	2.0	14.3	-6.0	-8.89	-3.19	-9.02	-3.92	5.88	6.00
8	1.8	0.6	100.0	2.1	47.6	-6.0	-9.96	-4.24	-10.01	-4.39	6.30	6.30
9	1.8	0.6	3.0	1.2	1.4	-7.0	-8.06	-2.37	-8.47	-4.64	4.51	4.70
10	1.8	0.6	10.0	1.7	4.8	-7.0	-8.96	-3.26	-9.18	-4.48	5.51	5.60
11	1.8	0.6	30.0	2.0	14.3	-7.0	-9.89	-4.19	-10.02	-4.70	6.00	6.00
12	1.8	0.6	100.0	2.1	47.6	-7.0	-10.96	-5.24	-11.01	-5.33	6.30	6.30
13	1.8	0.6	3.0	1.2	1.4	-8.0	-9.06	-3.37	-9.47	-5.28	4.51	5.00
14	1.8	0.6	10.0	1.7	4.8	-8.0	-9.96	-4.26	-10.18	-5.21	5.54	5.60
15	1.8	0.6	30.0	2.0	14.3	-8.0	-10.89	-5.19	-11.02	-5.60	6.00	6.00
16	1.8	0.6	100.0	2.1	47.6	-8.0	-11.96	-6.24	-12.01	-6.29	6.30	6.30

Columns: (1) Model number; (2) Primary mass (M_\odot); (3) Secondary mass (M_\odot); (4) SMA separation (AU); (5) Bondi-Hoyle accretion radius (AU); (6) Outer boundary of the disk (AU); (7) Mass loss rate from primary ($M_\odot \text{ yr}^{-1}$); (8) Accretion rate into disk ($M_\odot \text{ yr}^{-1}$); (9) Total mass that goes through the disk in 0.5 Myrs (M_\odot); (10) Accretion rate onto the star ($M_\odot \text{ yr}^{-1}$); (11) Disk mass at steady state (M_\odot); (12) Time to achieve steady state (yrs); (13) Simulation run time (yrs). Columns 7-13 are shown in logarithmic scale.

dio sources at cm wavelengths (Taylor & Seaquist 1984). These systems would be classified as symbiotic stars (Kenyon 1986).

Despite their much lower accretion rates, the central star accretes a larger fraction of infalling material in wide binaries. For $a \approx 3\text{--}100$ AU, the Bondi-Hoyle accretion radius R_a exceeds R_{st} the stagnation radius where the flow velocity in the disk changes sign. Thus, some fraction of infalling material flows out through the disk. The rest accretes onto the central star. In these simulations, the ratio of accreted to ejected material ranges from roughly 55% for close binaries ($a = 3$ AU) to $\sim 80\%$ for wide binaries ($a = 100$ AU). The accretion flow in the accretion disk is bimodal. Generally, material at separations somewhat shorter than R_A flows into the star; the rest of the material outflows out into the extended disk up to R_{out} and is eventually ejected from the disk.

Accreted material typically has a negligible impact on the central MS star. For typical lifetimes of 10^5 yr or

less, the central star accretes less than 1% of its initial mass. In the closest binaries with the highest mass loss rates, the accretor may accrete from 10% to 90% of its initial mass over the lifetime of the companion (e.g. see the overall accreted mass assuming steady state, over 0.5 Myr, $\dot{M}_{disk}^{0.5}$; Table 1). Although our models do not account for the mass increase of the secondary in these cases, the disk achieves steady-state long before the MS star accretes a significant amount of mass. Thus, our steady-state disks still correctly represent the likely physical state of the system.

Accreted material has a more significant impact on accreting white dwarfs. Aside from their visibility as symbiotic stars, wind-fed disks surrounding white dwarfs can produce a variety of eruptive phenomena (Kenyon 1986). At low accretion rates, cold white dwarfs undergo degenerate shell flashes and become classical novae (Kenyon & Truran 1983). White dwarfs accreting at larger rates yield non-degenerate flashes

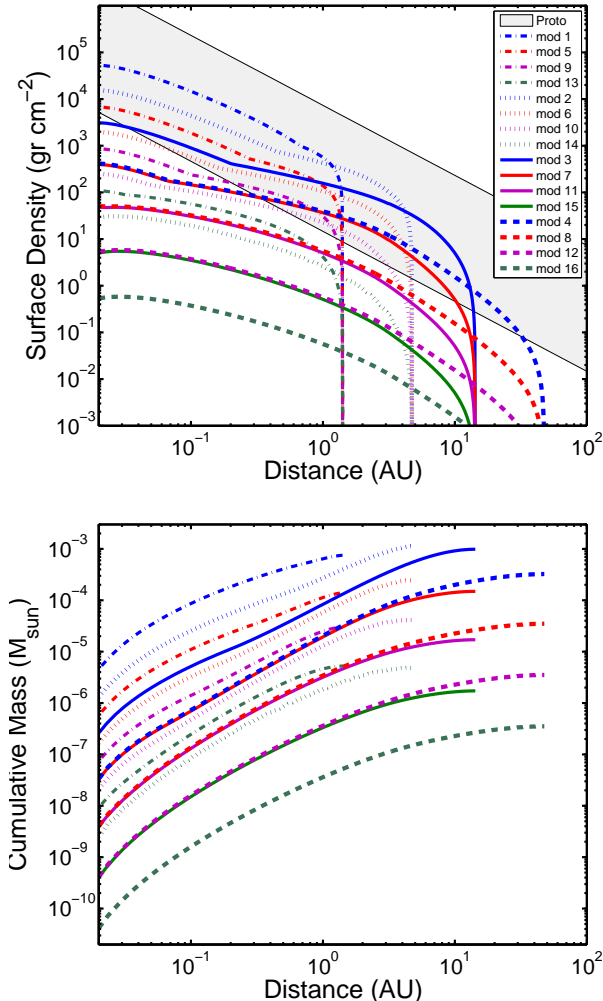


FIG. 2.— Radial profile of wind accretion disks at steady state. Top: The radial density profiles of wind accretion disks under various conditions. Also shown is a shaded region corresponding to a range of protoplanetary disk models which only differ in their overall normalization corresponding to the range of total disk masses as inferred from observations ($\sim 2 \times 10^{-4} - 10^{-1} M_{\odot}$; mean of $2 \times 10^{-3} M_{\odot}$; Andrews & Williams 2007). Bottom: The cumulative mass radial profile of wind accretion disks. Lines correspond to the same models in Fig. 1 (described in Table 1).

as in the symbiotic stars V1016 Cyg and HM Sge (Mikolajewska & Kenyon 1992). In some systems, the rates are sufficient to allow the white dwarf to evolve close to the Chandrasekhar limit and become a type Ia supernova (Starrfield et al. 2005).

Steady-state surface density profiles generally follow expectation. Over the entire disk, the surface density approximately scales with radius as $\Sigma \propto r^{-n}$, with $n \approx 0.8-1.5$. The normalization of the surface density scales almost linearly with the accretion rate into the disk. Changes in slope typically occur in the inner disk, when the disk becomes hot enough to evaporate dust grains, and in the outer disk, when the energy generated by irradiation or infall dominates the energy generated by viscosity (e.g., Chambers 2009, and references therein).

We briefly explored the effect of different viscosity parameters on the overall structure and mass of the disks (see table 1). In general, the steady state disk mass is roughly inversely proportional to α , and scales linearly

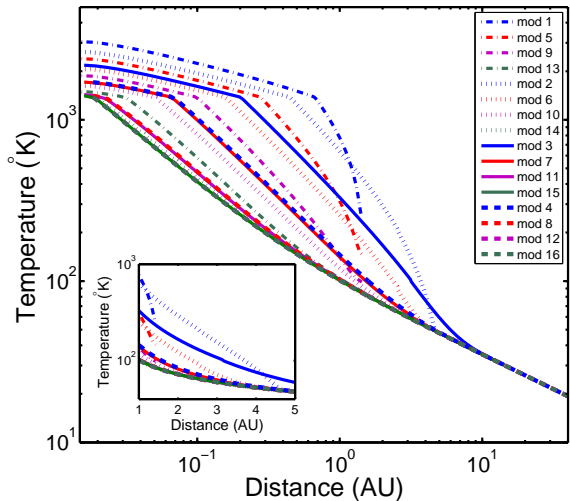


FIG. 3.— Radial temperature profile of wind accretion disks (inset shows a zoom up region; note linear distance-scale). The radial temperature profiles of wind accretion disks under various conditions are shown; the lines correspond to similar models as described in Fig. 1. Note that regions in which temperatures rise beyond approximately 1000 K might be susceptible to thermal disk instability, not modeled here.

with α^{-1} . These results hold as long as the disk is cold. As the disk gets hotter, more of the disk has an opacity dependent temperature which slightly changes the relation, but the overall behavior is close to linear. Beside the different overall scaling, the disk spatial structure is very similar.

Steady-state temperature profiles are generally shallower than steady-state accretion disks fed by a lobe-filling companion (Lynden-Bell & Pringle 1974). In most steady disks, the effective temperature of the disk scales with radius as $T \propto r^{-m}$, with $m \approx 0.75$. For wind-fed disks in very wide binaries at very low accretion rates, the steady-state slope approaches the standard $m \approx 0.75$. As the binary separation contracts and the wind accretion rate grows, the temperature profile becomes more shallow. For the closest binaries, our results suggest $m \approx 0.4$. The range in the slope is small, from $m \approx 0.4$ in close binaries with large accretion rates to $m \approx 0.7$ in wide binaries with small accretion rates. Thus, the temperature profile scales very weakly with the separation or the mass loss rate of the primary star.

5. DISCUSSION

The results from the calculations lead to several broad conclusions. Physical properties of wind-fed accretion disks depend on the orbital separation and the evolutionary state (mass loss rate) of the primary star. When the secondary is a main sequence star, it is observable only when the binary is close and the primary is an AGB star. Otherwise, wind-fed accretion has few, if any, direct observational consequences. When the secondary is a white dwarf, the binary is almost always observable as a symbiotic star.

Although optical/UV spectroscopic observations are sufficient to detect luminous symbiotic stars (Kenyon 1986), direct imaging can often reveal the binary companion. In Mira B, IUE spectroscopic observations first identified emission from a hot white dwarf accret-

ing material from the Mira wind (Reimers & Cassatella 1985), recent HST observations resolved the system and detected the accretion disk directly (Ireland et al. 2007). For a derived binary separation of ~ 70 AU, the inferred accretion luminosity of $\sim 10^{-10} M_{\odot} \text{yr}^{-1}$ (Sokoloski & Bildsten 2010) is roughly consistent with our models. High resolution imaging of other symbiotic-like binaries, including R Aqr and CH Cyg, would provide additional tests of these calculations.

Aside from producing interesting symbiotic stars, WD accretors in wide binaries can accrete enough material to approach the Chandrasekhar limit (Table 2; Starrfield et al. 2005; Shen & Bildsten 2007, and references therein). If these WDs grow, they are susceptible to traditional type Ia supernovae (Arnett 1996) and to sub-Chandrasekhar Helium detonation supernovae (e.g. Woosley et al. 1986; Bildsten et al. 2007; Perets et al. 2010; Waldman et al. 2011). In most simulations, the growth of the white dwarf depends on the way material is accreted. Thus, understanding the structure of the disk is important for understanding whether wind-fed white dwarfs are good SNe progenitors. Our disk models provide a step along the path to understanding these outcomes.

Wind-fed disks around white dwarfs provide a less traditional connection to other astrophysical systems. For separations of 3 – 100 AU and mass loss rates of $10^{-8} - 10^{-5} M_{\odot}^{-1}$, wind-fed disks have surface density and temperature profiles similar to those observed in low-mass protoplanetary disks. For comparison, Fig. 2 shows the range of surface density profiles inferred for an ensemble of protoplanetary disks in nearby star-forming regions (Andrews & Williams 2007; Chiang & Youdin 2010). The shaded region corresponds to disks with masses of $\sim 2 \times 10^{-4} - 10^{-1} M_{\odot}$. With typical lifetimes of a few Myr, physical processes in protoplanetary disks yield planets on short timescales. Given the similar lifetimes of AGB mass-losing primary stars, it is plausible that some aspects of planet formation occur in the wind-fed disks of wide binary systems (Perets 2010a,b).

Despite the similarity in instantaneous disk masses, disks in wide binaries have a distinct advantage over protoplanetary disks in producing planets. Continuous feeding by the primary star guarantees that the total mass available for planet formation is, in principle, larger for wide binaries than for protoplanetary disks. In close binaries with evolved AGB primaries, the total mass accreted by the central star is at least as large as the most protoplanetary disk. Thus, massive planets could grow in many of these disks.

Testing this idea is challenging. The most massive disks in wide binaries are not as large as those in protoplanetary disks; dust emission from the AGB primary complicates acquiring the submm and mm observations required to estimate dust masses. Occasional nova eruptions

may also frustrate the coagulation processes that grow dust grains from the Mira wind into the planetesimals that produce planets. However, ALMA has sufficient resolution to detect structures in the disks of wide binaries. Identifying structures similar to those in protoplanetary disks might allow robust comparisons between the grain properties and the profiles of surface density and temperature. Detection of debris disks around nearby white dwarfs suggests that planets (or debris from planets) survive the evolution from a main sequence star into a white dwarf (e.g., Kilic et al. 2012). The frequency of wide WD companions to WD debris disks provides some estimate for the likelihood of this ‘second generation’ planet formation scenario.

6. SUMMARY

Using a set of numerical calculations, we have explored the evolution and long term steady state structure of wind-accretion disks in wide evolved binaries ($a \approx 3 - 100$ AU). These systems evolve rapidly (see Fig. 1) and achieve a steady state on timescales which are typically much shorter than typical stellar evolution timescales of $\sim 10^5$ yr. During steady state, disks have similar surface density and temperature profiles with total masses of a few $\times 10^{-5} - 10^{-3} M_{\odot}$. The radial density profile is a broken power law in the inner regions and an exponential decline at the outer edge where the disk is truncated by tidal forces from the companion. The radial temperature profile is also described by a broken power law but does not decline dramatically at the outer edge of the disk.

Understanding the formation, structure, and evolution of wind-fed accretion disks is important for a wide variety of phenomena in evolved wide binary systems, including chemically peculiar stars, novae, supernovae, stellar outbursts, and symbiotic binaries. In close binary systems with evolved AGB primaries, significant accretion from a wind-fed disk provides a natural mechanism for chemical enrichment and abundance anomalies in otherwise normal main sequence and white dwarf stars. Over a broad range of separations and mass loss rates, wind-fed accretion onto white dwarfs can produce nova eruptions and, possibly, supernova eruptions. By providing a foundation for relating the mass loss rate of evolved red giants to the temperature and luminosity of the companion, our results also enable more detailed studies of the physical structure of individual binary systems.

Our analysis begins to make a link between the disks in evolved binaries and protoplanetary disks. The structure and evolution of both types of disks depends on uncertain physics, including the disk viscosity and interactions between stellar photons and disk material. For most accretion rates, large disks often drive massive winds which may interact with the surrounding wind from the primary (in a binary system) or a molecular cloud (in a protostellar system). Observational comparisons among disks with similar accretion rates and sizes might improve our overall understanding of accretion phenomena.

REFERENCES

- Alexander, R. D. & Armitage, P. J. 2009, *ApJ*, 704, 989
 Alexander, R. D., Clarke, C. J., & Pringle, J. E. 2006, *MNRAS*, 369, 216
 Alexander, R. D., Wynn, G. A., King, A. R., & Pringle, J. E. 2011, *MNRAS*, 418, 2576
 Andrews, S. M. & Williams, J. P. 2007, *ApJ*, 671, 1800
 Arnett, D. 1996, *Supernovae and Nucleosynthesis: An Investigation of the History of Matter from the Big Bang to the Present*, ed. Arnett, D.
 Bath, G. T. & Pringle, J. E. 1981, *MNRAS*, 194, 967

- . 1982a, *MNRAS*, 199, 267
 —. 1982b, *MNRAS*, 201, 345
 Bildsten, L., Shen, K. J., Weinberg, N. N., & Nelemans, G. 2007, *ApJ*, 662, L95
 Bromley, B. C. & Kenyon, S. J. 2011, *ApJ*, 735, 29
 Busso, M. et al. 2001, *ApJ*, 557, 802
 Cannizzo, J. K., Smale, A. P., Wood, M. A., Still, M. D., & Howell, S. B. 2012, *ApJ*, 747, 117
 Chambers, J. E. 2009, *ApJ*, 705, 1206
 Chiang, E. & Youdin, A. N. 2010, *Annual Review of Earth and Planetary Sciences*, 38, 493
 Chiang, E. I. & Goldreich, P. 1997, *ApJ*, 490, 368
 D'Alessio, P., Canto, J., Calvet, N., & Lizano, S. 1998, *ApJ*, 500, 411
 de Val-Borro, M., Karovska, M., & Sasselov, D. 2009, *ApJ*, 700, 1148
 Duquennoy, A. & Mayor, M. 1991, *A&A*, 248, 485
 Eggleton, P. P. 1983, *ApJ*, 268, 368
 Hadjidemetriou, J. D. 1963, *Icarus*, 2, 440
 Han, Z. et al. 1995, *MNRAS*, 277, 1443
 Hueso, R. & Guillot, T. 2005, *A&A*, 442, 703
 Ireland, M. J. et al. 2007, *ApJ*, 662, 651
 Kenyon, S. J. 1986, *The symbiotic stars* (Cambridge and New York, Cambridge University Press, 1986, 295 p.)
 Kenyon, S. J. & Hartmann, L. 1987, *ApJ*, 323, 714
 Kenyon, S. J. et al. 1991, *AJ*, 101, 637
 Kenyon, S. J. & Truran, J. W. 1983, *ApJ*, 273, 280
 Kenyon, S. J. & Webbink, R. F. 1984, *ApJ*, 279, 252
 Kenyon, S. J., Webbink, R. F., Gallagher, J. S., & Truran, J. W. 1982, *A&A*, 106, 109
 Kilic, M., Patterson, A. J., Barber, S., Leggett, S. K., & Dufour, P. 2012, *MNRAS*, 419, L59
 Livio, M., Soker, N., de Kool, M., & Savonije, G. J. 1986, *MNRAS*, 222, 235
 Luck, R. E. & Bond, H. E. 1991, *ApJS*, 77, 515
 Lynden-Bell, D. & Pringle, J. E. 1974, *MNRAS*, 168, 603
 Mastrodemos, N. & Morris, M. 1998, *ApJ*, 497, 303
 McClure, R. D. & Woodsworth, A. W. 1990, *ApJ*, 352, 709
 Mikolajewska, J. & Kenyon, S. J. 1992, *MNRAS*, 256, 177
 Noebauer, U. M., Long, K. S., Sim, S. A., & Knigge, C. 2010, *ApJ*, 719, 1932
 Olofsson, H., González Delgado, D., Kerschbaum, F., & Schöier, F. L. 2002, *A&A*, 391, 1053
 Perets, H. B. 2010a, arXiv:1012.0572
 —. 2010b, arXiv:1001.0581
 Perets, H. B. et al. 2010, *Nature*, 465, 322
 Pringle, J. E. 1981, *ARA&A*, 19, 137
 Ramstedt, S., Schöier, F. L., Olofsson, H., & Lundgren, A. A. 2006, *A&A*, 454, L103
 Reimers, D. & Cassatella, A. 1985, *ApJ*, 297, 275
 Ruden, S. P. & Lin, D. N. C. 1986, *ApJ*, 308, 883
 Ruden, S. P. & Pollack, J. B. 1991, *ApJ*, 375, 740
 Shen, K. J. & Bildsten, L. 2007, *ApJ*, 660, 1444
 Siviero, A. et al. 2009, *MNRAS*, 399, 2139
 Soker, N. & Rappaport, S. 2000, *ApJ*, 538, 241
 Sokoloski, J. L. & Bildsten, L. 2010, *ApJ*, 723, 1188
 Sokoloski, J. L., Luna, G. J. M., Mukai, K., & Kenyon, S. J. 2006, *Nature*, 442, 276
 Starrfield, S. et al. 2005, *Nuclear Physics A*, 758, 455
 Stepinski, T. F. 1998, *Icarus*, 132, 100
 Taylor, A. R. & Seaquist, E. R. 1984, *ApJ*, 286, 263
 Waldman, R. et al. 2011, *ApJ*, 738, 21
 Wang, Y.-M. 1981, *A&A*, 102, 36
 Webbink, R. F. et al. 1987, *ApJ*, 314, 653
 Woosley, S. E., Taam, R. E., & Weaver, T. A. 1986, *ApJ*, 301, 601